IOP Conf. Series: Materials Science and Engineering **174** (2017) 012038 doi:10.1088/1757-899X/174/1/012038

Analysis of squeeze film process between non-parallel circular surfaces

A V Radulescu and I Radulescu

Department Machine Elements and Tribology, POLITEHNICA University of Bucharest, Spl. Independentei 313, Bucharest, Romania

E-mail: varrav2000@yahoo.com

Abstract. The purpose of the paper is to determine the performance of a Newtonian fluid, in the case of squeezing process between non-parallel circular surfaces, from theoretical and experimental point of view. The theoretical analysis is based on the two-dimensional Reynolds equation, which is solved assuming the simplifying hypothesis of the "narrow bearing theory". With this approximation, it is possible to neglect certain terms in the Reynolds equation, and an analytical expression for the pressure distribution on the superior surface can be written. The theoretical results have been compared with the experimental determination of the pressure distribution, obtained on a modified Weissenberg rheogoniometer. For the squeezing experiment, two oils specific for internal combustion engines have been used. Their viscosity was measured with a con and plate Brookfield viscometer. The stand has the possibility to measure the pressure variation with the film thickness, in three points, for different squeezing velocity and for an imposed geometry of the circular plates. In conclusion it can observe a good correlation between theory and experiment, in the case of thick lubricant films. At low values of the thickness of lubricant film, the theoretical model has to be improved, using finite theory method for flow modelling.

1. Introduction

Squeezing phenomenon describes the large deformation (or a flow) of a soft material (or a viscous fluid) between two solid surfaces approaching one to each other. During squeezing the gap between surfaces is changing in time and the sample is ejected from the gap. In many applications the gap is small in comparison to the other dimensions of the surfaces, in particular discs diameters, so squeezing flow is mainly associated to thin film hydrodynamics, lubrication and rheology of complex fluids, [1]. The interest shown to this complex flow is due to various applications: the presence of this motion in mechanical engineering [2], rheology [3], constructions [4], industrial processes [5], biological processes such as mastication [6] etc.

The purpose of the present paper is to use the squeezing process for an engineering application, in particular for the analytical approximate formulation of the squeeze film process between non-parallel circular surfaces. The theoretical results are validated on an experimental stand, based on a modified Weissenberg rheogoniometer.

2. Theoretical model

The theoretical analysis is based on a generalized model for any incompressible flow, the Newtonian model, for squeezing the film between two non-parallel circular surfaces (figure 1):

$$\tau = \eta \frac{du}{dy} \tag{1}$$

where: τ - shear stress;
η - viscosity;
u - velocity;
x, y, z - Cartesian coordinates.

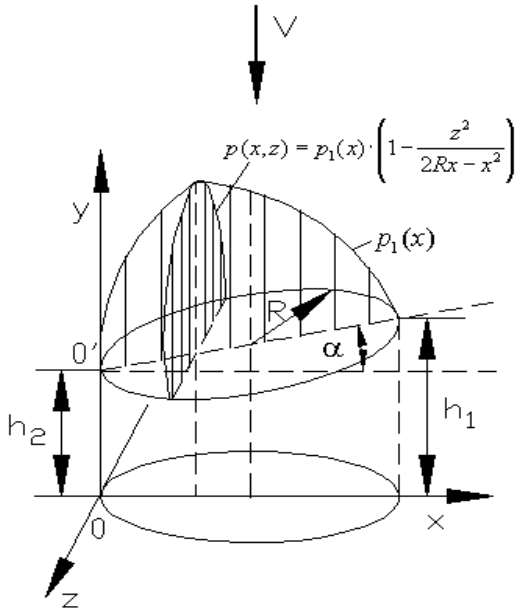

Figure 1. Geometry of the interstice.

The geometry of the interstice is characterized by the equation:

$$h(x) = h_2 + x \cdot \mathrm{tg}\alpha\ ,\ x \in [0, 2R] \tag{2}$$

where: h - film thickness;
h_2 - minimum film thickness;
α - tilted angle;
R - radius.

The main hypotheses of the flow are:

- the flow is laminar, incompressible and stationary;
- the oil viscosity is constant on the film thickness;
- the tilted angle α is very small ($\alpha \leq 1^0$).

In order to determine the pressure distribution, the two-dimensional Reynolds equation for non-parallel surfaces is considered:

$$\frac{d}{dx}\left(h^3 \frac{dp}{dx}\right) + \frac{d}{dz}\left(h^3 \frac{dp}{dz}\right) = -12\eta V \tag{3}$$

where: p - pressure; V - squeezing velocity.

The analytical solution for equation (3) is obtained assuming the simplifying hypothesis of the "narrow bearing theory" [7], [8], [9]. According to this theory, the pressure variation across the Oz axis is much greater than that along Ox axis. With this approximation, it is possible to neglect certain terms in the Reynolds equation, and an analytical expression for the pressure variation on the superior surface can be written down.

By integrating equation (3) and imposing the limit conditions ($p_1(x)$ = 0 for x = 0 and 2R), the expression of the pressure distribution corresponding to Ox axis can be obtained:

$$p_1(x) = \frac{6\eta V}{tg^2\alpha}\left[\frac{1}{h(x)} - \frac{h_1 h_2}{h(x)^2\left(h_1 + h_2\right)} - \frac{1}{h_1 + h_2}\right] \tag{4}$$

where: h_1 - maximum film thickness.

Regarding this equation for the pressure distribution corresponding to Ox axis (equation 4), an important observation is imposed: due to the fact that the tilted angle α appears at the denominator, when α = 0, apparently the pressure $p_1(x)$ leads to infinite. Actually, taking into account the expression of definition for the film thickness (equation 2), which also depends on tilted angle α, and calculating the limit value for the pressure $p_1(x)$, the following calculus expression is obtained:

$$\lim_{\alpha \to 0} p_1(x) = \frac{3\eta V\left(2Rx - x^2\right)}{h_2^3} \tag{5}$$

which is independent of the tilted angle α.

For the Oz axis, considering the simplifying theory of the narrow bearing, the pressure distribution becomes:

$$p_2(z) = p_1(x)\left(1 - \frac{z^2}{2Rx - x^2}\right) \tag{6}$$

Finally, from the equations (4) and (6), results the two-dimensional pressure distribution:

$$p(x,z) = \frac{6\eta V}{tg^2\alpha}\left[\frac{1}{h(x)} - \frac{h_1 h_2}{h(x)^2\left(h_1 + h_2\right)} - \frac{1}{h_1 + h_2}\right]\left(1 - \frac{z^2}{2Rx - x^2}\right) \tag{7}$$

Of course, the same observation done for the equation (4), regarding the tilted angle α when α = 0, is also available for equation (7).

Figures 2 and 3 show two cases of the spatial pressure distribution in the fluid film, corresponding to two cases of the tilted angle: parallel surfaces ($\alpha = 0^0$) and non-parallel surfaces ($\alpha = 0.5^0$).

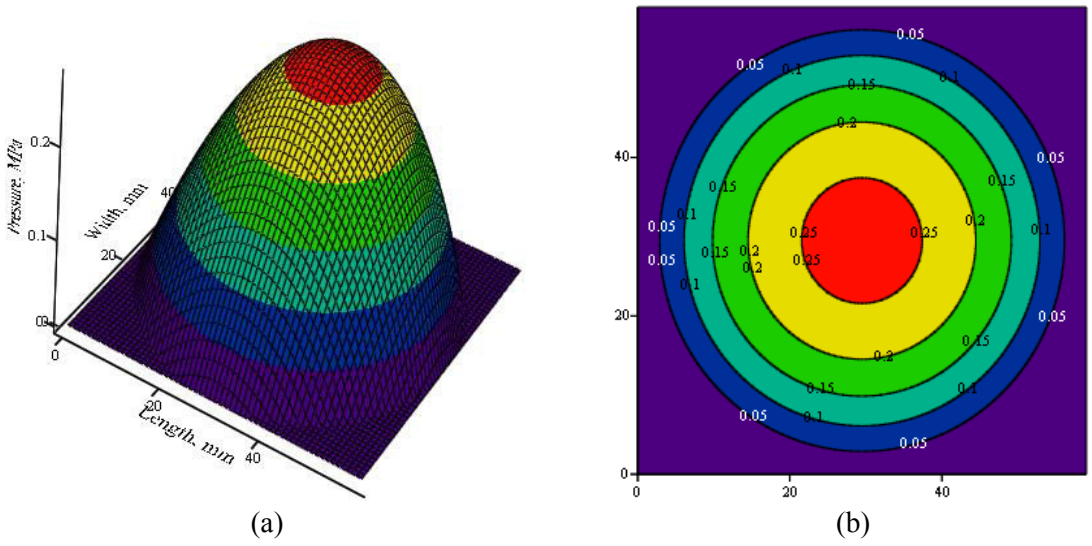

(a) (b)

Figure 2. Spatial pressure distribution for parallel surfaces: 3D pressure distribution (a) and isobar curves (b) ($\alpha = 0^0$, η = 0.2 Pa·s, R = 30 mm, V = 0.5 mm/s, h_2 = 0.1 mm)

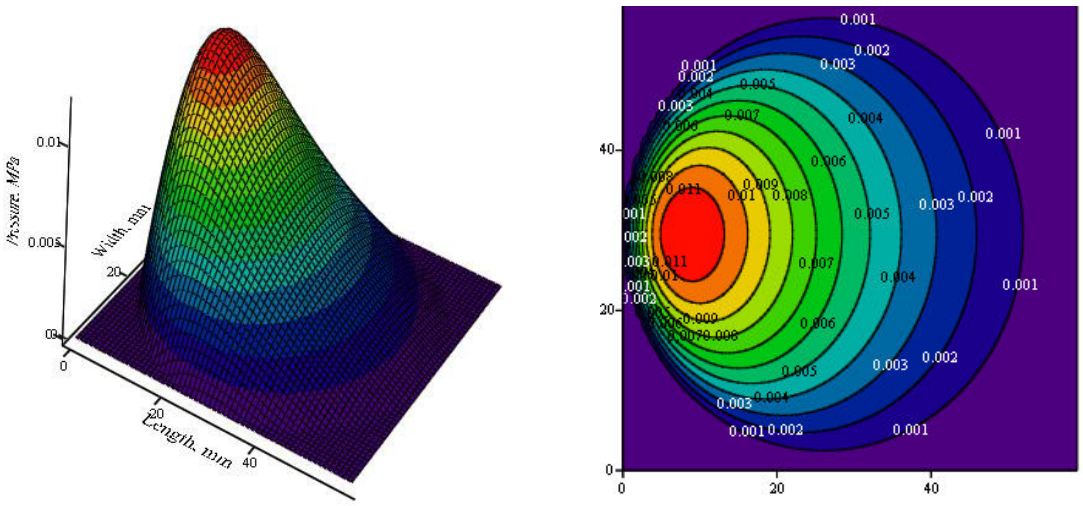

(a) (b)

Figure 3. Spatial pressure distribution for non-parallel surfaces: 3D pressure distribution (a) and isobar curves (b) ($\alpha = 0.5^0$, $\eta = 0.2$ Pa·s, $R = 30$ mm, $V = 0.5$ mm/s, $h_2 = 0.1$ mm)

Figure 4 shows the pressure distribution along the Ox axis, for different values of the tilted angle, in order to put in evidence the values of the maximum pressure and the corresponding axial coordinate.

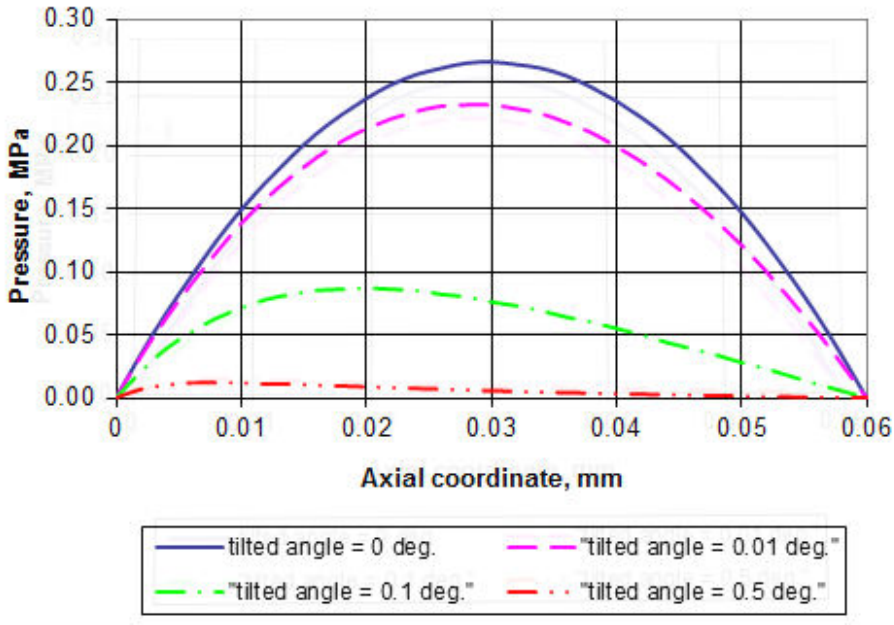

Figure 4. Pressure distribution along Ox axis.

It can be observed the difference between the shapes of the pressure distribution in the two cases, and also between the values of the maximum pressure in the film (0.25 MPa for parallel surfaces and 0.011 MPa for non-parallel surfaces).

According to this observation, the tilted angle between the surfaces has an important influence on the pressure distribution. Any deviation from parallelism of the surfaces has a major importance concerning the flow of the lubricant between the surfaces and the maximum pressure that occurs.

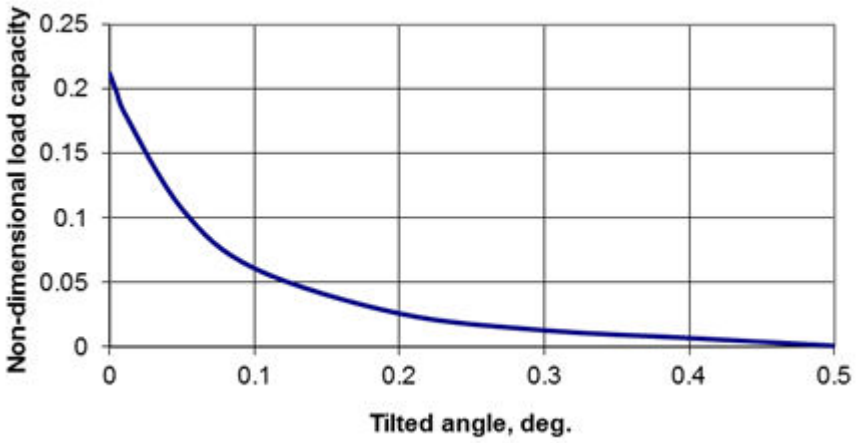

Figure 5. Non-dimensional load capacity versus tilted angle.

The load capacity F is obtained by numerical integration of the pressure distribution, following the relation:

$$F = \iint_S p(x,z)dzdx \tag{8}$$

where S is the integrating surface given by:

$$S: \quad (x-R)^2 + z^2 \le R^2 \tag{9}$$

The variation of the non-dimensional load capacity $\overline{F} = \dfrac{Fh_2^3}{6\pi\eta VR^4}$ as function of the tilted angle α is presented in figure 5.

The same influence of the tilted angle on the load capacity can be observed, same as for the pressure distribution.

3. Experimental stand

The experimental stand used for the carrying out of the determinations was a modified rheogoniometer Weissenberg (figure 6), built up from the main structural elements:

- Central working unit;
- Testing couple, which consists on two circular paralel surfaces;
- Driving system of the superior disc, corresponding to the friction couple;
- Electric and comand system for the servomotor;
- Pressure transducers;
- Displacement transducer;
- Data acquisition system.

For the acquisition and the numerical treatment of the experimental data it has been used the LabVIEW software. The measurement of the signal provided by the three pressure transducers and the displacement transducer was realized using an acquisition board NI USB-6008. The pressure transducers have been calibratated with a 200 g load, finally obtaining conversion relations between electrical signal and pressure, respectively displacement. Figure 7 presents a detail regarding the construction and the location of the pressure transducers.

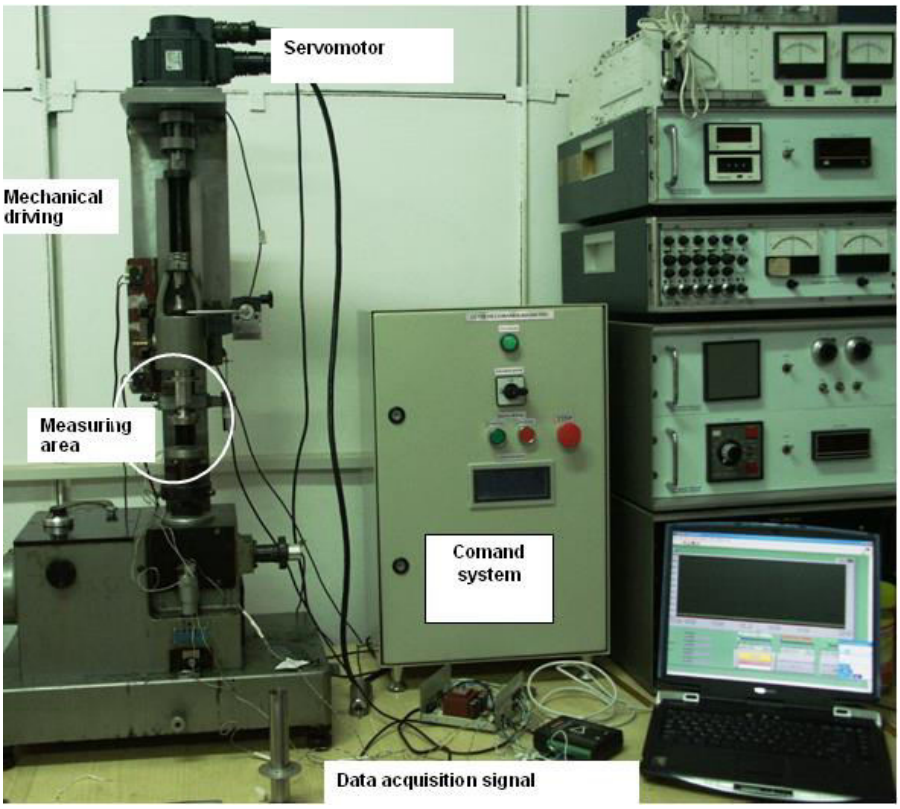

Figure 6. General view of the experimental stand.

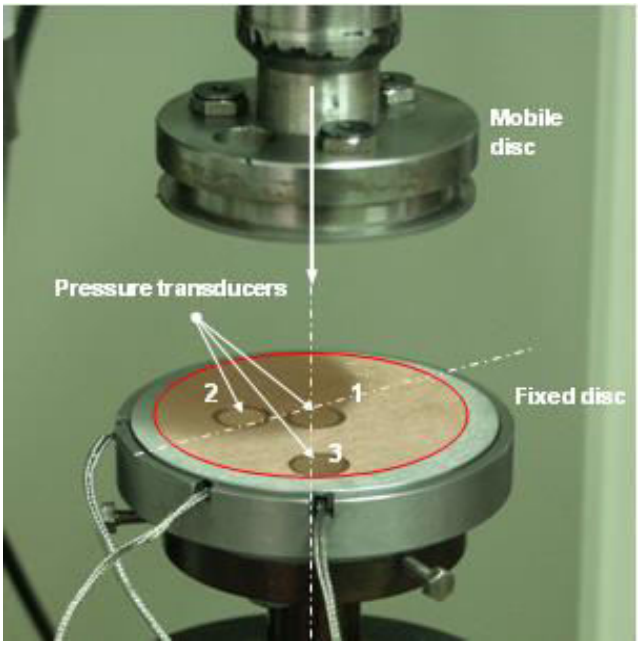

Figure 7. Location of the pressure transducers.

For the squeezing experiment, two oils have been used: 10W40 oil, with the dynamic viscosity η = 0.2 Pa·s, and M30 oil, characterized by the dynamic viscosity η = 0.5 Pa·s. The viscosity was measured at 20^0C, with a con and plate Brookfield viscometer.

The geometry of the surfaces is characterized by the radius of the circular plate (R = 30 mm) and the positions of the pressure transducers:

- Central transducer, with the coordinates $x = R$ and $z = 0$;

- Median transducer, with the coordinates $x = 5/6 \cdot R$ and $z = \sqrt{3}/6 \cdot R$;
- Lateral transducer, with the coordinates $x = 1/3 \cdot R$ and $z = 0$;

For the testing protocol, four velocities of the superior disc have been imposed (0.25, 0.50, 0.75 and 1 mm/s), and the film thickness varied from 0.6 to 0.1 mm. The stand has the possibility to measure the pressure variation with the film thickness, for different squeezing velocity and for an imposed geometry of the circular plates.

4. Results and discussions

In the first stage, the data obtained from the acquisition system were plotted in a pressure – film thickness diagram, for each three transducers, and they were correlated with the theoretical values obtained from equation (6), for $\alpha = 0^0$ (case of the parallel surfaces).

Analysing the experimental results, it has been observed a significant difference between theory and experiment. The explanation of this phenomenon consists in the existence of a deviation from parallelism between the superior and the inferior surfaces (tilted angle $\alpha > 0^0$).

Figure 8 shows the position of the pressure transducers on the inferior surface and the correspondence with the theoretical pressure distribution, for two values of the tilted angle: $\alpha = 0^0$ and $\alpha = 0.1^0$. The difference between the two analysed cases consists in the fact that in the second case, the transducer 1 (central) and transducer 2 (median) show the same pressure.

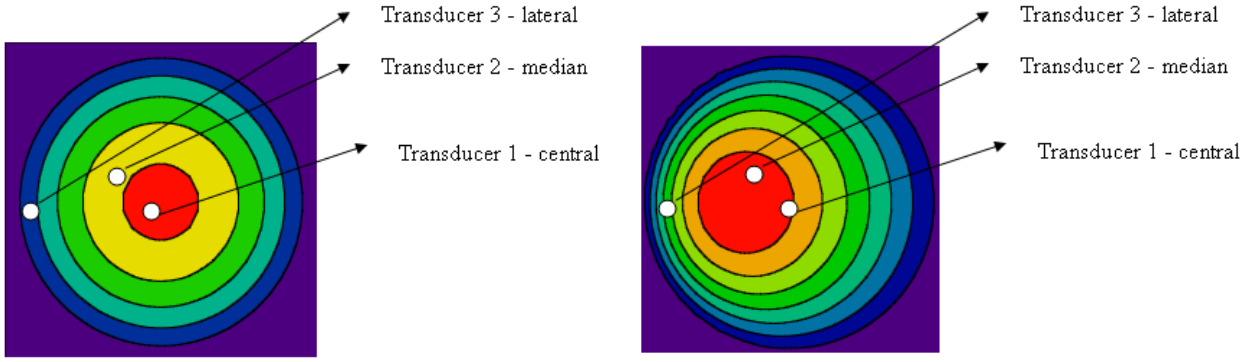

(a) (b)

Figure 8. Correspondence between pressure transducers and pressure distribution for $\alpha = 0^0$ (a) and $\alpha = 0.1^0$ (b)

In the second stage, in order to correlate the experimental results with the theory, the measured values of the pressure and film thickness were plotted together with the theoretical curves for different tilted angles. These results, obtained for the two tested oils, are presented in figures 9 and 10.

5. Conclusions

1. A theoretical model for the squeeze film process between non-parallel circular surfaces has been developed and the theoretical results have been validated using an experimental stand;
2. The pressure distribution for the non-parallel surfaces is strong influence by the tilted angle;
3. The proposed model is in a good agreement with the experiment for mean values of the film thickness (0.1 … 0.5 mm);
4. For lower values of the film thickness, the theoretical model has to be improved using the finite element methods for the modelling of the flow;
5. The geometry of the friction couple is not stable and the tilted angle between surfaces vary during the experiments.

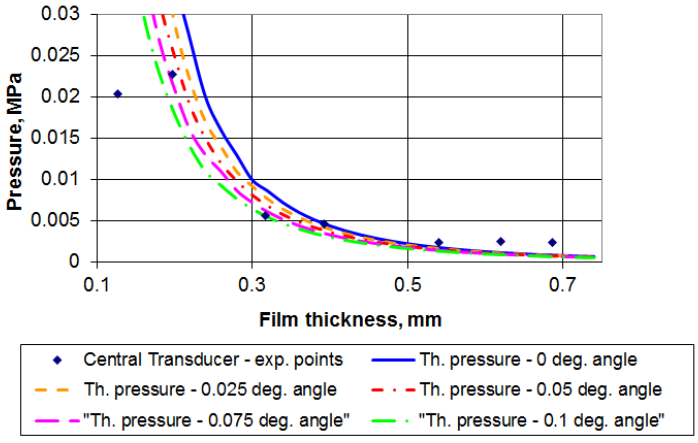

(a)

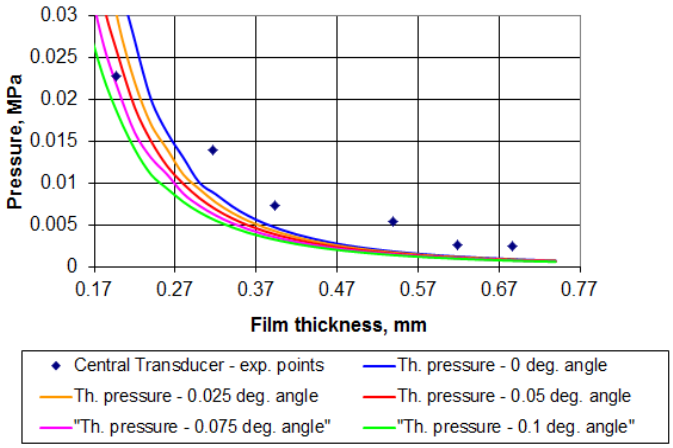

(b)

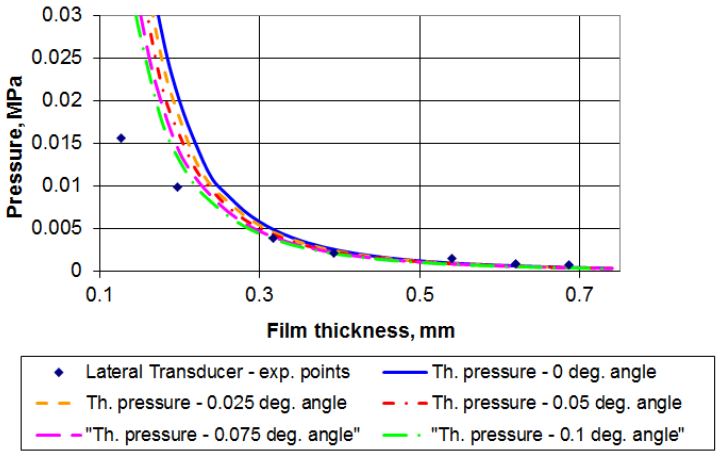

(c)

Figure 9. Experimental and theoretical results for 10W40 oil, in case of central transducer (a), median transducer (b) and lateral transducer (c)

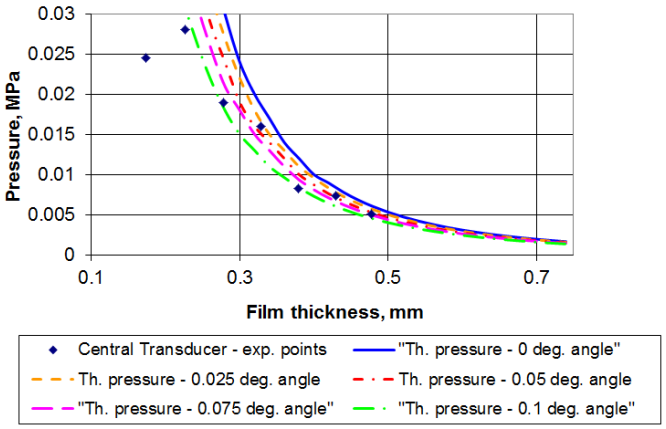

(a)

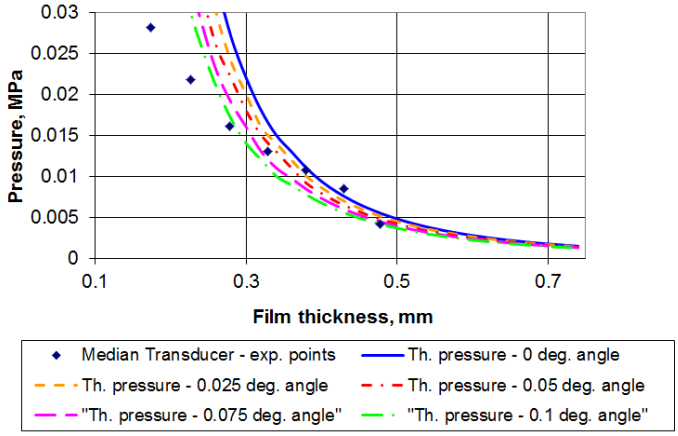

(b)

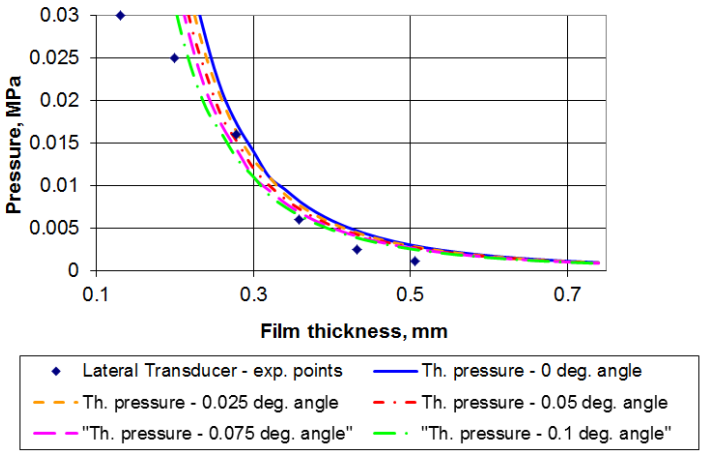

(c)

Figure 10. Experimental and theoretical results for M30 oil, in case of central transducer (a), median transducer (b) and lateral transducer (c)

References

[1] Engmann J, Servais C and Burbidge A 2005 *J. Non-Newtonian Fluid Mech.* **132** 1
[2] Debbaut B and Thomas K 2004 *J. Non-Newtonian Fluid Mech.* **124** 77
[3] Kolenda F, Retana P, Racineux G and Poitou A 2003 *Powder Technol.* **130** 56

[4] Toutoua Y, Roussela N and Lanos C 2005 *Cem. Concr. Res.* **35** 1891
[5] Kompani M and Venerus D C 2000 *Rheol. Acta* **39** 441
[6] Jiang P, See H, Swain M V and Phan-Thien N 2003 *Rheol. Acta* **42** 118
[7] Goenka P K and Oh K P 1986 *J. Tribol.* **108** 294
[8] Vignolo G G, Barilà D O and Quinzani L M 2011 *Tribol. Int.* **44** 1089
[9] Bezvani M A and Hahn E J 1993 *J. Tribol.* **115** 545